

Not All Pixels Are Equal: Learning Pixel Hardness for Semantic Segmentation

Xin Xiao, Daiguo Zhou, Jiagao Hu, Yi Hu, Yongchao Xu

Abstract—Semantic segmentation has recently witnessed great progress. Despite the impressive overall results, the segmentation performance in some hard areas (e.g., small objects or thin parts) is still not promising. A straightforward solution is hard sample mining, which is widely used in object detection. Yet, most existing hard pixel mining strategies for semantic segmentation often rely on pixel's loss value, which tends to decrease during training. Intuitively, the pixel hardness for segmentation mainly depends on image structure and is expected to be stable. In this paper, we propose to learn pixel hardness for semantic segmentation, leveraging hardness information contained in global and historical loss values. More precisely, we add a gradient-independent branch for learning a hardness level (HL) map by maximizing hardness-weighted segmentation loss, which is minimized for the segmentation head. This encourages large hardness values in difficult areas, leading to appropriate and stable HL map. Despite its simplicity, the proposed method can be applied to most segmentation methods with no and marginal extra cost during inference and training, respectively. Without bells and whistles, the proposed method achieves consistent/significant improvement (1.37% mIoU on average) over most popular semantic segmentation methods on Cityscapes dataset, and demonstrates good generalization ability across domains. The source codes are available at <https://github.com/Menoly-xin/Hardness-Level-Learning>.

Index Terms—Semantic segmentation, hard sample mining, pixel hardness learning, convolutional neural network

1 INTRODUCTION

SEMANTIC segmentation aims to assign a semantic label to each pixel in an image, and is one of the fundamental tasks in computer vision. Benefiting from some large-scale open-sourced semantic segmentation datasets [1]–[3] and developments of backbone networks [4]–[7], numerous studies have made impressive progress in the field of semantic segmentation. Specifically, since FCN [8] shed new light on pixel-wise prediction in an end-to-end manner using a fully convolutional neural network, enormous efforts have been devoted to developing new dense prediction style segmentation architectures. For example, PSPNet [9] fuses multi-scale feature maps for more sophisticated feature representation. The DeepLab family [10]–[12] enlarges receptive field via atrous spatial pyramid pooling (ASPP). Recently, many studies [13]–[25] resort to the attention mechanism for gathering more context information from the whole image for better semantic segmentation.

These methods effectively boost the performance of semantic segmentation by a large margin. Yet, most of them mainly frame the segmentation task as individual pixel-wise classification tasks, calculating the loss value for each pixel and then equally-weighted averaging the loss values to get an image-level loss. Such a scheme ignores that the difficulty

in classifying various pixels in an image is quite different. In fact, semantic segmentation is with a structured output. Many pixels are relatively easy to segment. The area with a complex structure deserves more attention for both manual annotation and segmentation. Therefore, a straightforward idea is to apply larger weights to harder pixels in averaging the pixel-wise loss values.

Over the past several years, the topic of focusing more on hard samples during training has attracted great research interest [26]–[28] in object detection. Existing methods [26]–[28] typically rely on current loss values to characterize the hardness of different samples, and only make use of hard samples with large loss values for training [26] or assign larger loss weights to samples with larger loss values [27], [28]. These hard sample mining methods effectively address the problem of extremely unbalanced hard and easy samples, achieving impressive results in object detection.

Different from object detection, to the best of our knowledge, hard pixel mining is not widely used in semantic segmentation. Directly applying hard pixel mining strategies based on current pixel loss values [26]–[28] to semantic segmentation may even harm the segmentation performance. In fact, thanks to the strong memorization ability of deep neural networks [29], the segmentation network is capable to well fit most pixels during training. Only a very few pixels around object boundaries have large loss values (see the top row of Fig. 1). Yet, it is usually ambiguous to accurately distinguish these pixels around boundaries even for manual annotation. The up-sampling operation in segmentation network further makes it ambiguous to discriminate these pixels for segmentation. The training focused on these ambiguous pixels may lead to degenerated segmentation results. Therefore, trivially paying more attention to pixels with large loss values is not very effective.

- X. Xiao and Y. Xu are with National Engineering Research Center for Multimedia Software, Institute of Artificial Intelligence, School of Computer Science, and Hubei Key Laboratory of Multimedia and Network Communication Engineering, Wuhan University, Wuhan, 430070, China. (E-mail: {xinxiao, yongchao.xu}@whu.edu.cn).
- D. Zhou and J. Hu are with Xiaomi AI Lab, Wuhan, 430070, China. (E-mail: {zhoudaiguo, hujiaogao}@xiaomi.com).
- Y. Hu is with Hubei Medical Devices Quality Supervision and Test Institute, Hubei Center for AI Medical Devices Supercomputing, Wuhan, 430070, China. (E-mail: huyi@whmit.cn).

Corresponding author: Yongchao Xu

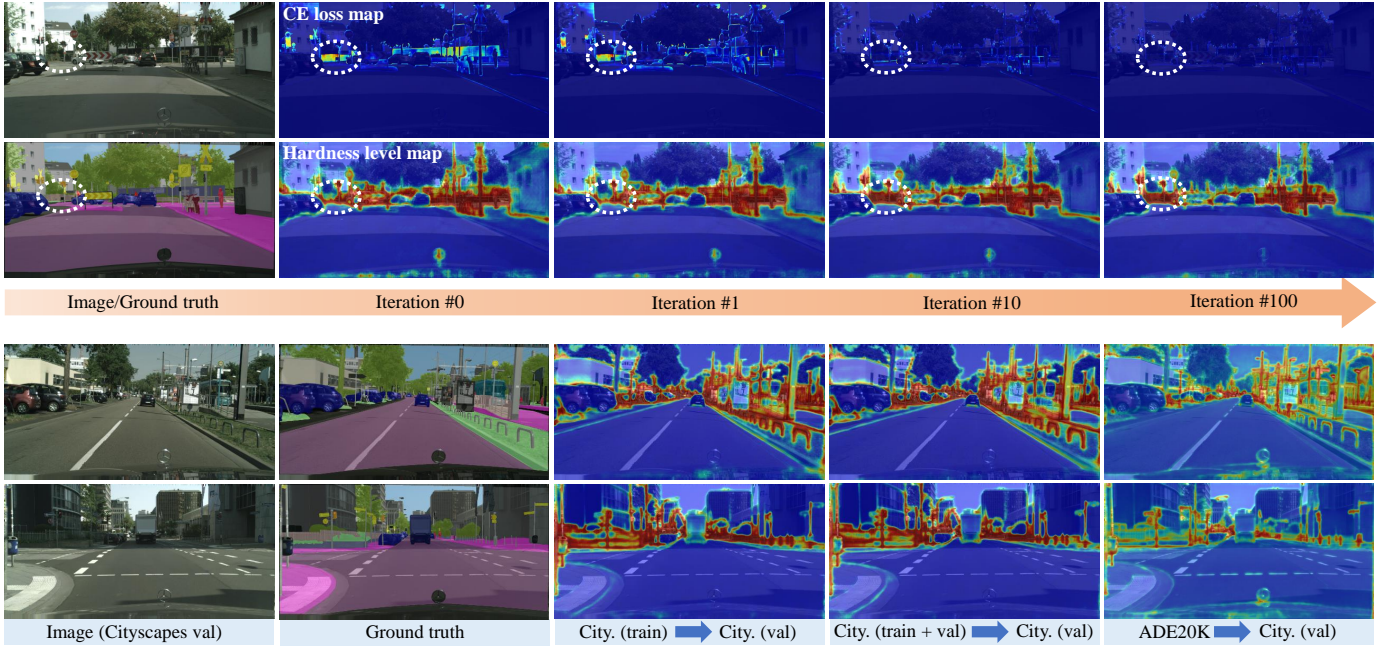


Fig. 1. Visualization of cross-entropy loss maps and learned hardness level (HL) maps at different iterations (top two rows) of continuing to train the model (well trained on Cityscapes training set) on an image in the validation set of Cityscapes. The bottom two rows show some learned HL maps on images in the validation set of Cityscapes using three models trained on Cityscapes training set, Cityscapes training and validation set, and ADE20K training set. The learned HL maps are related to inherent image structure, and are thus quite and generalize well.

There exist some semantic segmentation methods [30]–[37] that consider the difference of segmentation difficulty for different pixels in a more sophisticated way. Specifically, some methods [30], [31] regard regions with confident (having large maximum scores of predicted probability) segmentation results as easy regions and unconfident regions as hard regions, and then apply different segmentation heads for hard and easy regions. Some other methods select hard regions based on loss values [32] or an object detection network [33], and then zoom in the selected hard regions for refined segmentation. In medical image segmentation, some methods adopt an extra segmentation loss on non-discontinuity areas [34] or regions with anatomically implausible segmentation results based on adversarial confidence learning [35] or topological analysis [36], [37]. Taking into account the difference of segmentation difficulty among pixels [30]–[37] have been proven useful in improving segmentation results.

In this paper, different from the existing methods, we propose to learn pixel hardness for semantic segmentation. More precisely, instead of relying on the current loss values for extracting hard regions, we propose to duplicate the segmentation head for learning a hardness level (HL) map, based on which we minimize a hardness-weighted segmentation loss for the segmentation head. Since there is no ground-truth for the pixel hardness, the key lies on how to learn an appropriate hardness level map. For that, we control the maximum relative ratio between the largest and smallest hardness level among all pixels by applying a Sigmoid operation and adding a small constant value. Besides, we also normalize the sum of harness level over all pixels to 1. This also acts as a hardness level competition among pixels, avoiding only a few overwhelming pixels with large hardness level. We then maximize the hardness

weighted segmentation loss for optimizing the HL branch. Since deep neural networks usually quickly fit easy samples and gradually fit hard samples [38], maximizing the hardness-weighted segmentation encourages larger hardness level on pixels with larger historical loss values. As illustrated in the bottom two rows of Fig. 1, this leads to a stable and meaningful hardness level map, which is related to the image structure and thus generalizes well to unseen images. Paying more attention to pixels with larger hardness level results in improved segmentation results. Note that the HL branch is only involved in training phase and has independent gradient flow with the segmentation head.

The main contribution of this paper is three-fold: 1) We propose a novel idea of learning pixel hardness for semantic segmentation, subtly making use of the difference of difficulty in segmenting different pixels; 2) We develop an effective scheme in learning the hardness level map without explicit ground-truth, yielding stable and meaningful hardness level map which generalizes well to unseen images; 3) Without bells and whistles, the proposed method achieves consistent/significant improvements over most semantic segmentation methods on various types of images, and demonstrates great potential in semi-supervised and domain-generalized semantic segmentation.

2 RELATED WORK

2.1 Semantic segmentation

Semantic segmentation has been studied for a long time [39]. The pioneering work FCN [8] firstly introduces fully convolutional networks and renders the segmentation task end-to-end manner, opening up new avenues for semantic segmentation. Since then, numerous efforts have been devoted to developing convolutional segmentation methods. For

instance, some early studies [10], [40] adopt structured operators (*e.g.*, conditional random fields) to refine segmentation results, but at the price of a substantial increase in inference cost. Some following works [9], [11], [12], [41]–[45] design advanced segmentation architectures for better feature representation. For example, PSPNet [9] fuses multi-scale features by pyramid pooling module. DeepLab series [11], [12] adopts atrous spatial pyramid pooling to enlarge receptive field. Since the introduction of attention mechanism to the vision task [13], numerous studies [13]–[25] have focused on this topic. Most of them mainly employ the non-local operator or the attention mechanism for gathering semantic context information across the whole image. Some methods [46]–[48] attempt to improve the segmentation accuracy by better aligning boundary or leverage boundary-related features. Recently, transformer-based semantic segmentation methods [49], [50] have also attracted much attention and achieved impressive segmentation results.

With the impressive development of segmentation architectures, backbone networks also evolve rapidly. Since AlexNet [51] brings computer vision into a new era, convolutional neural networks serve as commonly used backbones throughout recent computer vision tasks. Many convolutional backbone networks (*e.g.*, VGG [4], ResNet [5], Res2Net [52], HRNet [53]) being deeper and more effective have been proposed. Besides, compact and efficient backbone networks (*e.g.*, MobileNet [54], EfficientNet [6]) which require much less running cost have also been proposed, making it possible to deploy convolutional neural networks on low-performance equipment. More recently, some vision transformers [7], [55], [56] greatly boost segmentation performance. The CNN-based network ConvNeXt [57] with modern components also achieves comparable performance with some vision transformers.

Benefiting from these advanced studies, semantic segmentation has witnessed considerable progress. Yet, most studies equally consider each pixel in segmentation, ignoring that the difficulty for segmenting each pixel in an image is quite different. The proposed method learns the pixel hardness for semantic segmentation, effectively making use of the difference of segmentation difficulty among pixels. The proposed method can be plugged to most semantic segmentation methods, improving the performance with ignorable extra training cost and no extra cost during test.

2.2 Hard sample mining

Some early studies [26]–[28] have noticed that the difficulty of classifying different samples in an image is quite different in the field of object detection. They adjust the weights for different samples based on their loss values. For example, OHEM [26] only picks out hard samples with high loss values for training, which can be viewed as assigning 0 weight for the other easy samples with small loss values. Focal loss [27] assigns much larger weights for hard samples with higher loss values, and much smaller weights for easy samples with lower loss values. These hard mining strategies have made impressive progress in object detection. Yet, to the best of our knowledge, there does not exist a widely used loss-value-based weighting method specifically designed for semantic segmentation.

In the field of semantic segmentation, there are also some works [30]–[37] follow the spirit of hard sample mining. For instance, Li *et al.* [30] present a deep layer cascade method that adopts shallow (*resp.* deep) network for easy (*resp.* hard) regions with large (*resp.* small) maximum scores of predicted probability. The work in [31] applies three segmentation heads for coarse segmentation, segmentation on hard and easy regions also based on the maximum score of predicted probability. The segmentation results of the three heads are then fused together to generate the final segmentation. OHRM [32] and NightLab [33] first extract hard regions based on loss values [32] or an detection network [33], then zoom in the extracted hard regions for re-training [32] or segmentation refinement in both training and testing [33].

Some medical image segmentation works [34]–[37] perform hard pixel mining by assigning larger loss weights to harder areas. For instance, Nie and Shen [35] rely on adversarial confidence learning by using a discriminator on the segmentation output to find hard regions from the aspect of shape structure, and then apply a difficulty-aware attention mechanism on the hard regions. In [34], the authors propose to simply add extra loss in non-discontinuity areas. The studies in [36], [37] attempt to locate topologically important areas via topological analysis of the segmentation output, and apply extra loss on these areas. These works in [34], [36], [37] are equivalent to assigning larger loss weights on hard regions given by non-discontinuity or topologically important areas.

The works in [26], [27], [34]–[37] are the most related works for the proposed method. Different from [26], [27] that characterize the hardness based on current loss values, the proposed method automatically learns the pixel hardness and makes use of historical and global loss values, leading to more appropriate loss weights and better segmentation performance. Compared with [34]–[37] which aim to segment medical objects often having specific prior shapes, the proposed method is more general and able to segment objects in natural images whose shape structure varies much more than medical objects.

3 PROPOSED METHOD

3.1 Overview

Existing semantic segmentation methods mainly adopt equally-weighted average loss for all pixels in an image to get the image-level loss. This ignores that the difficulty in segmenting each pixel in an image is different, which also holds for manual annotation. Based on this, a straightforward idea is to apply different loss weights for pixels of different hardness. Indeed, the hard sample mining strategy which assigns higher loss weights for samples with higher loss values, has been proven very useful in object detection [26]–[28]. Yet, to the best of our knowledge, the effective hard sample mining in object detection is not widely used in semantic segmentation. Directly adopting such hard pixel mining usually yields degenerated segmentation results. In fact, deep neural networks have extraordinary memorization ability [29], and are capable of memorizing almost all training samples. This results in very few pixels with large loss values during the segmentation training. Most of these pixels with large loss values lie around object boundary (see

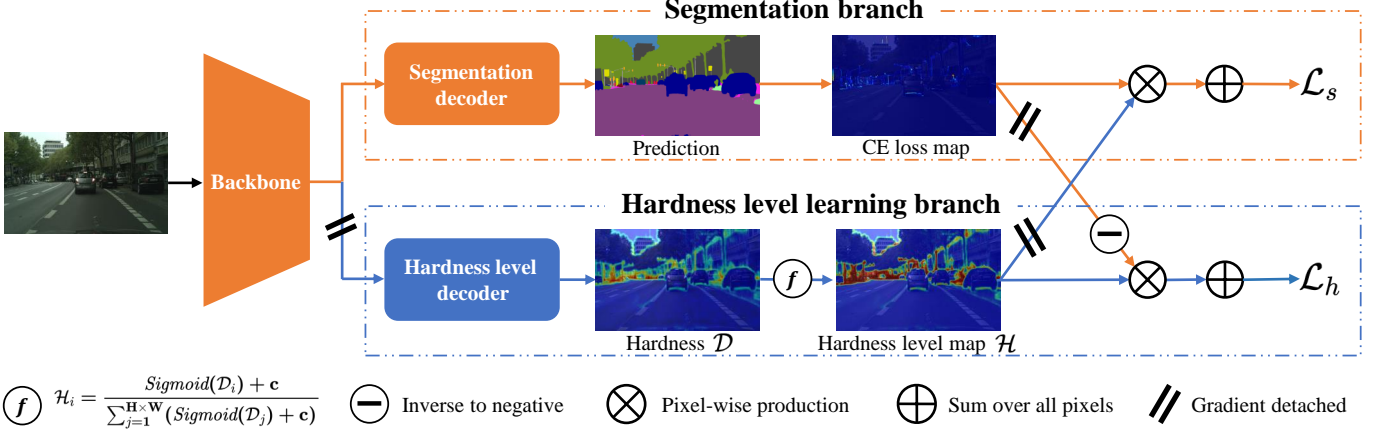


Fig. 2. The pipeline of the proposed pixel hardness learning method. The hardness level learning branch shares the same network architecture as the segmentation head, and only works during training phase and thus requires no cost during testing phase. Note that the gradient flow separately propagates along the corresponding branch (the path of the same color), avoiding the gradient interaction between the two branches.

Fig. 1), where it is often ambiguous to distinguish different classes for both annotation and segmentation due to inevitable up-sampling operation. The optimization focused mainly on these few pixels may lead to a wrongly overfitted segmentation model. Therefore, the hardness based on current loss value is not effective for semantic segmentation.

To better take into account the difference of segmentation difficulty, we propose to learn pixel hardness for semantic segmentation. Specifically, we propose a novel hardness level learning method to extract pixel hardness knowledge from the evolving historical pixel loss values. In fact, deep neural networks usually start to quickly fit easy samples and then gradually fit hard samples [38]. This fitting process contains rich information about pixel hardness. Based on this, we introduce an auxiliary hardness level (HL) learning branch, accumulating historical information. This branch is optimized by maximizing the hardness-weighted segmentation loss given by the multiplication of hardness level map and cross-entropy loss map. Such an optimization scheme encourages to assign high hardness values for pixels with large loss values in the training process, and makes use of the global and historical pixel loss values. This results in a stable and meaningful hardness level map related to the inherent structure of an image (see Fig. 1). For the segmentation branch, we minimize the hardness-weighted segmentation loss. Note that the segmentation branch and HL learning branch have independent gradient flow during optimization in training. The HL learning branch is only involved during training, and thus requires no extra cost in inference. The overall pipeline is depicted in Fig. 2.

3.2 Pixel hardness learning

The mainstream semantic segmentation methods mainly adopt a backbone convolutional neural network to extract multi-scale features, followed by a segmentation head composed of several convolution layers. The segmentation usually relies on a 1×1 convolution layer for pixel-wise classification, using equally averaged cross-entropy loss over all pixels. This ignores that the segmentation difficulty for different pixels is not equal for both manual annotation and

segmentation. Indeed, during annotation, we usually pay more attention to complex areas. The segmentation network first quickly fits easy pixels, and then gradually fits hard pixels [38]. We propose to make use of this property to learn pixel hardness for semantic segmentation. The key lies on how to learn the hardness level (HL) map without direct and explicit ground-truth supervision. We detail the network architecture and training objective in the following.

Network architecture for HL learning: In addition to the segmentation head, we introduce an auxiliary hardness level learning branch on the extracted multi-scale feature of the backbone network. For the sake of simplicity, we simply adopt the same network architecture as the segmentation head by changing the output channel to 1 for learning pixel hardness \mathcal{D} . As depicted in Fig. 2, we apply a transformation on the hardness \mathcal{D} to obtain the final hardness level map. Specifically, we apply a Sigmoid function on \mathcal{D} to make it into range $[0, 1]$. This avoids negative hardness and too large overwhelming hardness. Besides, we also add a constant weight c to the output of Sigmoid function, avoiding some pixels being neglected for too small \mathcal{D} . In fact, the constant c in $\mathcal{Z} = \text{Sigmoid}(\mathcal{D}) + c$ acts as a hyper-parameter that sets lower/upper bound for pixel hardness level, and controls the maximal relative hardness ratio between different pixels. This further prevents overwhelming hardness for some pixels. We then divide \mathcal{Z} by the sum of \mathcal{Z} over all pixels in the image, yielding the final hardness level map \mathcal{H} . Formally, for the i -th pixel, the final hardness level \mathcal{H}_i is given by:

$$\mathcal{H}_i = \frac{\mathcal{Z}_i}{\sum_{j=1}^{H \times W} \mathcal{Z}_j} = \frac{\text{Sigmoid}(\mathcal{D}_i) + c}{\sum_{j=1}^{H \times W} (\text{Sigmoid}(\mathcal{D}_j) + c)}, \quad (1)$$

where H and W stand for the height and width of the image, respectively. This normalization makes the sum of the hardness level over all pixels equal 1, acting also as a competition mechanism for hardness levels among all pixels in the image. A high hardness level for a pixel relatively limits the hardness level for the other pixels.

Note that the auxiliary hardness level learning branch is detached (see Fig. 2). In this way, the extra branch does not influence the shared backbone for segmentation branch.

Training objective for HL learning: Since there is no ground-truth for the hardness level, the key of HL learning lies on how to design an appropriate training objective. Considering that deep neural networks usually begin to quickly fit easy samples and then gradually fit hard samples during training process, the pixel-wise cross-entropy loss values of classical segmentation loss \mathcal{L} quickly converge to small values for easy pixels, and keep relatively large in many training iterations for hard pixels (see the first row in Fig. 1). Therefore, the historical pixel-wise cross-entropy loss values \mathcal{L} during training process encodes the pixel hardness information. Based on this, we propose to minimize the following loss for the HL learning branch:

$$\mathcal{L}_h = - \sum_{i=1}^{H \times W} \mathcal{H}_i \times \mathcal{L}_i^d, \quad (2)$$

where \mathcal{L}^d denotes the gradient detached cross-entropy loss \mathcal{L} . As depicted in Fig. 2, the gradient flow of minimizing \mathcal{L}_h does not back-propagate to the segmentation branch, and only propagates along the auxiliary HL learning branch.

Minimizing the loss function in Eq. (2) is equivalent to maximize the hardness-weighted cross-entropy segmentation loss, which encourages high hardness level for hard pixels with large historical loss values. Specifically, the gradient of the loss function defined in Eq. (2) with respect to the hardness level is given by:

$$\frac{\partial \mathcal{L}_h}{\partial \mathcal{H}} = -\mathcal{L}^d. \quad (3)$$

From the aspect of gradient, since the cross-entropy loss value on each pixel is non-negative, minimizing the loss \mathcal{L}_h mainly leads to a competitive increase of hardness level for all pixels, on which the summation of hardness level equals 1 based on Eq. (1). A higher (*resp.* very small) pixel loss value triggers relatively larger (*resp.* ignorable) increasing of the hardness level on the corresponding pixel. Therefore, minimizing the loss function \mathcal{L}_h results in large (*resp.* small) hardness level for hard (*resp.* easy) pixels with relatively high (*resp.* low) historical pixel loss values. Besides, thanks to the Sigmoid operation and the hyper-parameter c in Eq. (1) that avoid overwhelming hardness for some pixels, the set of pixels with relatively large historical loss values would have high hardness level. This gives rise to relatively stable and meaningful hardness level related to the inherent structure of an image (see the second row of Fig. 1).

3.3 Hardness-aware semantic segmentation

The proposed pixel hardness learning can be applied to most popular semantic segmentation methods. We keep the segmentation head unchanged. Instead of classical equally-weighted cross-entropy loss used in most semantic segmentation methods, we propose to minimize the following hardness-weighted segmentation loss \mathcal{L}_s :

$$\mathcal{L}_s = \sum_{i=1}^{H \times W} \mathcal{H}_i^d \times \mathcal{L}_i, \quad (4)$$

where \mathcal{H}^d stands for the gradient detached hardness level map. As shown in Fig. 2, the gradient flow of minimizing \mathcal{L}_s

only back-propagates along the segmentation branch, and does not influence the hardness level learning branch.

The final overall loss \mathcal{L}_f for the whole model is given by.

$$\mathcal{L}_f = \mathcal{L}_s + \alpha \times \mathcal{L}_h, \quad (5)$$

where α is a hyper-parameter that scales the learning rate for the hardness level learning branch. Based on Eq. (2) and Eq. (4), the hardness level learning and segmentation branch are separately optimized. The α controls the increasing rate of competing hardness level on each pixel during training.

4 EXPERIMENTS

4.1 Datasets and evaluation protocol

We conduct extensive experiments on Cityscapes [1] and ADE20K [2] for natural image segmentation, iSAID [3] and Total-Text [58] for aerial and text image segmentation, respectively. The details of these datasets are given as follows.

Cityscapes [1] is a high quality semantic segmentation dataset for urban scene understanding, which contains 5,000 finely annotated images (2,975, 500, and 1,525 for training, validation, and test set, respectively) and about 20,000 coarsely annotated images. Only the finely annotated are used in training for all experiments. We mainly report segmentation results on the validation set.

ADE20K [2] is a widely used scene parsing benchmark dataset containing pixel-wise annotations of 150 categories. This dataset is pretty challenging due to its numerous classes. The dataset provides 20,000 and 2,000 images for training and validation, respectively.

iSAID [3] is a large-scale aerial image dataset for semantic segmentation. This dataset contains 2,806 high-resolution images with segmentation annotations of 15 categories. The dataset is split into 1/2, 1/6, and 1/3 portion for training, validation, and test, respectively. Following the common practice, we cut the original high-resolution images into small patches, and report results on the validation set.

Total-Text [58] consists of 1,555 images with more than 3 different text orientations, including horizontal, multi-oriented, and curved. There are 1,255 and 300 images for training and testing, respectively. The annotations only contain two categories: foreground texts and background.

Evaluation protocol: We adopt the classical mean of class-wise intersection over union (mIoU) for all quantitative evaluation of segmentation performance.

4.2 Implementation details

The proposed method is implemented using the mmsegmentation [59] framework on a workstation with 8 NVIDIA Tesla A100 GPUs. We adopt the default settings (including batch size, number of iterations, crop size, test strategy, optimizer and related parameters for optimization, etc.) of mmsegmentation for all baseline methods and the proposed method. Unless explicitly stated, we follow the most common default settings (listed in Tab. 1) of mmsegmentation.

During training, we augment the training images with common data augmentation strategies, including random

TABLE 1

Training details and test strategy on different datasets. We adopt the same settings for the baseline methods and the proposed approach.

Dataset	Training details			Test strategy
	Batch size	#Iterations	Crop size	
Cityscapes [1]	8	40,000	769 × 769	Sliding
ADE20K [2]	16	160,000	512 × 512	Whole
iSAID [3]	16	80,000	896 × 896	Whole
Total-Text [58]	16	40,000	512 × 512	Whole

scaling between 0.5 and 2.0, random horizontal flipping, random cropping, and random color jittering.

In all experiments, the hyper-parameter c involved in Eq. (1) is set to 0.1. We set the hyper-parameter α involved in Eq. (5) to 0.01 for all experiments. Note that we report the semantic segmentation performance of *single scale* inference using the model of the last iteration for all baseline methods and the proposed method.

4.3 Analysis of learned hardness level map

We conduct three types of analysis on the learned HL maps. In the following, we first visualize the learned HL maps, followed by an analysis of the relation between HL maps and segmentation quality. We then show the generalization ability of HL map to unseen images.

Visualization of meaningful and stable HL maps: The proposed method aims to learn pixel hardness for semantic segmentation. We first visualize some learned HL maps for images in the training set of a model. As shown in Fig. 1 (second column from the right in bottom two rows) and Fig. 3 (top two rows), the learned HL maps have large values on complex areas, where they are difficult for segmentation and more attention should be paid for manual annotation. Therefore, the learned HL map is somehow meaningful and related to the inherent structure of an underlying image.

We also visualize how the HL map is learned during training. For that, we conduct an experiment by continuing to train a model (well-trained on Cityscapes training set) on an image in the validation set of Cityscapes for 100 iterations. As illustrated in Fig. 1 (top two rows), the cross-entropy loss values tend to decrease to very small values. The HL map is in general rather stable. Taking a closer look on the region within the white ellipse in Fig. 1, the HL values increase on pixels with relatively large historical pixel-wise cross-entropy loss values. Starting from the 10-th iteration in Fig. 1, almost all pixels have very low cross-entropy loss values. The learned HL map stays very stable from the 10-th iteration to the 100-th iteration. As explained in Sec. 3.2, such behavior of the HL map is reasonable based on Eq. (3) and Eq. (1). This implies that the proposed HL learning method effectively makes use of the historical loss values rather than current loss values, yielding a stable and meaningful HL map related to image structure.

Effectiveness of HL map in indicating hard pixels: The learned HL map is expected to be able to indicate hard pixels. To verify this, we evaluate the segmentation performance with respect to pixels with decreasing of HL

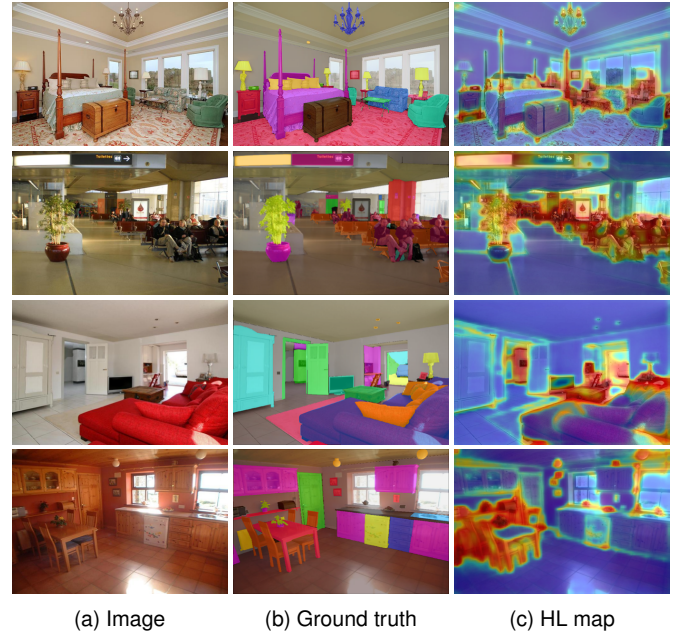


Fig. 3. Visualization of some learned hardness level maps for images in training (top two rows) and validation (bottom two rows) set of ADE20K.

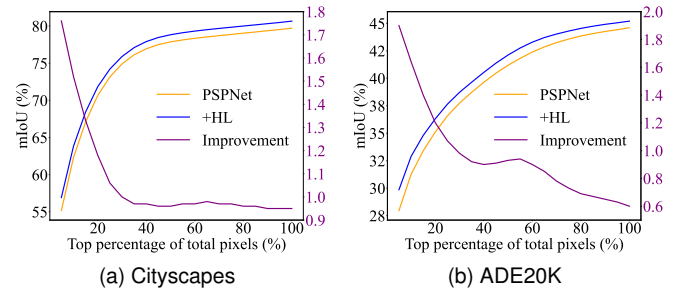


Fig. 4. Quantitative evaluation of applying the proposed pixel hardness learning method to the PSPNet [9] on different pixel subsets with decreasing hardness on the validation set of Cityscapes and ADE20K.

As depicted in Fig. 4, for both the ResNet-101-based baseline PSPNet [9] and the proposed method trained on the corresponding training set, the segmentation performance increases with respect to the decrease of learned HL on the validation set of Cityscapes and ADE20K, respectively. This implies that the learned HL map is effective in indicating hard pixels. Besides, since the validation images are not seen during training, this also implies that the proposed HL learning generalizes well to unseen images. It is noteworthy that the proposed hardness-aware semantic segmentation based on the learned HL map improves the segmentation performance more on hard pixels (see Fig. 4), further demonstrating the effectiveness of the learned HL map in indicating hard pixels.

Generalization ability of HL map to unseen images: The proposed HL learning branch is normally only involved in the training phase for semantic segmentation. Since the learned HL map is stable and meaningfully related to image structure. The learned HL map also generalizes well to unseen images. As shown in the middle column of the

TABLE 2

Quantitative benchmarks of applying the proposed method to some segmentation methods with different backbone networks (from lightweight to cumbersome) on the validation set of Cityscapes. * (*resp.* †) stands for training with 512×1024 (*resp.* 1024×1024) crop size, while testing on the whole image. SI: sidewalk; BU: building; TL: traffic light; TS: traffic sign; VE: vegetation; TE: terrain; PE: person; MO: motorcycle; BI: bicycle.

Backbone	Method	Road	SI	BU	Wall	Fence	Pole	TL	TS	VE	TE	Sky	PE	Rider	Car	Truck	Bus	Train	MO	BI	mIoU
ResNet-18 [5]	UPerNet [41]	97.72	82.36	91.80	55.57	56.47	60.35	63.80	74.00	91.82	63.79	94.32	78.84	57.06	94.20	64.94	83.77	71.22	57.25	74.21	74.39
	+HL	97.68	82.40	92.04	54.06	59.00	62.51	66.61	75.16	92.01	63.61	94.31	79.94	60.21	94.44	69.53	85.86	77.33	63.29	75.87	76.10 (+1.71)
HRNetV2P-W18 [53] (Small)*	OCRNet [42]	98.07	84.97	92.05	57.73	59.55	64.00	66.71	77.04	92.15	60.25	94.45	79.94	57.28	94.40	81.20	85.56	74.31	56.41	74.00	76.32
	+HL	97.99	84.81	92.15	53.18	61.73	66.26	69.63	77.10	92.40	62.50	94.14	81.62	59.76	94.80	81.64	87.66	77.35	61.76	76.83	77.54 (+1.22)
HRNetV2P-W18* [53]	OCRNet [42]	98.30	86.04	92.63	59.50	62.57	66.90	69.56	78.39	92.61	64.10	94.70	82.06	62.28	95.14	83.91	88.49	77.61	60.38	76.03	78.48
	+HL	98.24	86.09	92.98	59.10	65.07	69.02	71.84	79.29	92.90	64.59	94.82	83.57	64.97	95.26	80.59	88.61	76.92	63.11	77.99	79.21 (+0.73)
MobileNetV2* [54]	PSPPNet [9]	96.14	76.66	89.55	38.73	50.14	59.31	56.94	72.93	90.39	45.96	92.37	77.65	52.53	92.77	54.30	65.43	63.35	53.01	72.51	68.46
	+HL	96.09	74.72	90.41	48.54	48.68	60.76	61.82	73.70	90.88	49.31	92.65	78.68	54.04	93.11	48.38	68.24	65.22	53.41	73.95	69.61 (+1.15)
MobileNetV3* [60]	LRASPP [61]	97.44	80.92	90.49	53.36	52.82	57.24	56.56	69.06	91.44	61.12	93.86	74.65	49.02	92.63	59.04	75.34	56.50	50.99	70.87	70.18
	+HL	97.45	81.37	90.69	51.98	54.54	60.23	62.90	71.44	91.69	59.25	93.07	77.93	54.73	92.98	60.43	77.35	56.72	55.58	73.84	71.80 (+1.62)
BiSeNetV2† [44]	BiSeNetV2 [44]	98.01	83.45	91.94	57.69	56.75	60.68	66.67	76.17	92.04	62.01	94.67	79.42	56.58	94.29	68.62	73.61	42.90	56.31	73.60	72.92
	+HL	97.92	83.28	91.81	47.45	56.98	62.19	68.82	76.58	92.13	60.44	94.54	80.63	59.41	94.45	78.17	81.86	71.26	56.82	75.46	75.27 (+2.35)
ResNet-50 [5]	UPerNet [41]	97.85	83.52	92.90	61.76	60.95	64.28	70.36	78.66	92.52	65.79	94.96	81.78	62.51	95.02	66.09	87.97	79.64	66.32	77.58	77.92
	+HL	97.88	83.84	93.05	56.46	63.03	66.68	72.86	80.37	92.57	64.63	95.12	83.13	63.99	95.39	69.70	87.97	80.48	68.62	78.61	78.65 (+0.73)
ResNet-101 [5]	UPerNet [41]	98.12	85.10	92.95	59.59	63.82	65.89	71.63	79.47	92.64	64.27	95.00	82.38	62.40	95.14	72.98	88.23	81.65	66.22	78.07	78.71
	+HL	98.11	85.05	93.26	63.87	64.41	67.51	73.68	81.02	92.87	65.01	95.06	83.58	65.72	95.52	75.71	89.02	83.03	68.45	79.60	80.02 (+1.31)
HRNetV2P-W48* [53]	OCRNet [42]	98.29	85.86	93.32	58.99	64.57	69.55	73.18	81.28	92.97	66.43	95.09	83.94	65.47	95.70	81.79	92.16	82.48	69.41	78.68	80.48
	+HL	98.51	87.75	93.76	64.65	66.86	71.94	74.85	82.14	93.19	66.68	95.26	84.85	67.65	96.01	87.41	92.42	86.22	70.56	80.45	82.17 (+1.69)
ResNeXt-101 [62]	UPerNet [41]	98.18	85.42	93.28	63.12	65.80	67.68	72.95	80.90	92.78	66.06	95.13	83.86	66.35	95.64	76.03	89.42	83.92	67.66	79.17	80.18
	+HL	98.18	85.44	93.57	63.59	66.21	69.49	74.58	82.18	92.85	66.06	95.24	84.56	67.86	95.70	74.23	89.14	83.27	70.82	80.17	80.69 (+0.51)
ResNeSt-101 [63]	UPerNet [41]	98.09	84.75	93.14	64.03	63.35	66.13	71.19	80.21	92.73	65.08	95.08	82.80	63.68	95.38	73.43	86.90	82.01	67.16	78.04	79.11
	+HL	98.10	84.67	93.40	64.03	66.02	68.01	73.99	81.03	92.81	63.66	95.12	83.82	66.08	95.82	77.05	90.81	84.45	70.62	79.70	80.48 (+1.37)
ConvNeXt-Base [57]	UPerNet [41]	98.27	86.05	93.24	62.70	65.12	66.63	71.91	80.66	92.88	66.66	95.10	83.41	65.74	95.69	87.06	90.60	84.54	70.93	79.65	80.89
	+HL	98.29	86.33	93.43	62.85	65.67	68.06	73.61	81.39	93.05	66.87	95.14	84.12	66.74	95.91	85.18	91.33	84.94	72.27	80.14	81.33 (+0.44)

bottom two rows of Fig. 1 and the bottom two rows of Fig. 3, the proposed HL learning produces HL maps with similar structures on unseen validation images. Besides, as shown in the bottom two rows of Fig. 1, the model trained on the training and validation set of Cityscapes produces very similar HL maps with the model trained only on Cityscapes training set. This implies that the proposed HL learning generalizes well to unseen images. Furthermore, using the model trained on the ADE20K training set also yields similar HL maps (on Cityscapes validation images) as the model trained on Cityscapes training set, further demonstrating the good generalization ability of the proposed HL learning.

To quantitatively evaluate the generalization ability of the proposed HL learning, we compute the average of structural similarity (SSIM) [64] between HL maps given by different models on the Cityscapes validation set. Specifically, when applying the proposed method to the PSPNet [9] with ResNet-101 backbone, we achieve 0.95 SSIM between the model trained on both training and validation set of Cityscapes and the model trained only on Cityscapes training set. This suggests that the proposed HL learning generalizes well to unseen images of the same dataset. Moreover, we get 0.84 SSIM between the model trained on ADE20K training set and the model trained on Cityscapes training set, further demonstrating the good generalization ability of the proposed HL learning across datasets.

4.4 Experimental results

We conduct extensive experiments on four public datasets for semantic segmentation. Firstly, we apply the proposed method to different backbone networks and different base-

line segmentation methods on Cityscapes. This is followed by extensive experiments on ADE20K dataset using some popular baseline segmentation methods and backbone networks. We then evaluate the proposed method on iSAID and Total-Text dataset for aerial and text image segmentation, respectively. Some qualitative segmentation results are illustrated in Fig. 6. Applying the proposed HL learning approach to the baseline method is able to accurately segment the image, including the thin parts and small objects (within white ellipse of Fig. 6). The corresponding quantitative benchmarks on these datasets are given in the following.

Experimental results on Cityscapes: We first conduct two types of extensive experiments on Cityscapes dataset. The quantitative results of using different backbones and different segmentation architectures are detailed in the following.

Results of using different backbones: There are many different backbone networks (ranging from lightweight ResNet-18 [5] and MobileNet family [54], [60] to cumbersome ResNet-101 [5] and ConvNeXt [57]) for semantic segmentation. We mainly adopt widely used UPerNet [41] as the basic segmentation architecture for most backbones. For some specifically designed backbone networks, the adopted segmentation architectures in the corresponding original papers are used. The quantitative benchmark of applying the proposed HL learning method to different segmentation backbones is depicted in Tab. 2. The proposed method consistently or significantly outperforms the corresponding baseline methods. Specifically, the proposed method achieves in average 1.46% mIoU improvement on lightweight backbones, and 1.01% mIoU improvement on cumbersome backbones. It is noteworthy that the proposed method consistently/significantly

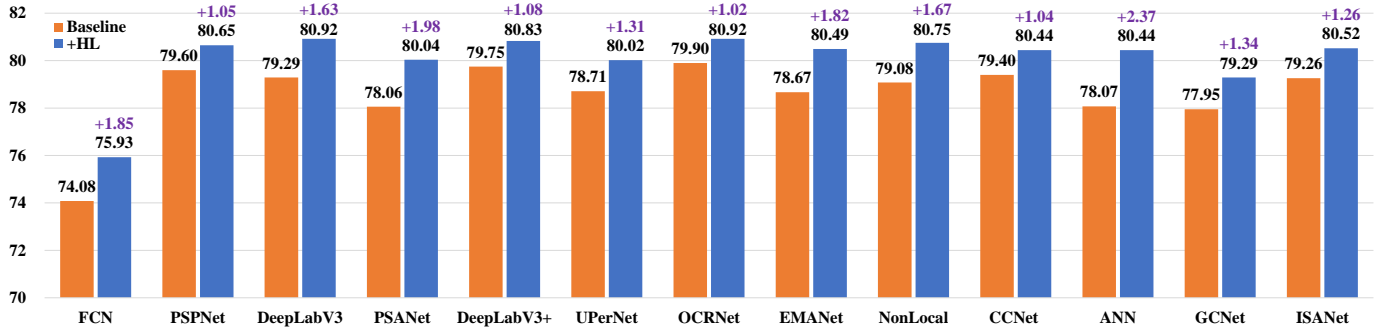


Fig. 5. Quantitative benchmark of applying the proposed pixel hardness learning method on different popular segmentation methods with ResNet-101 as the backbone network. The proposed method achieves consistent or significant improvements with no extra cost during inference.

TABLE 3

Quantitative evaluation of different popular methods on the validation set of ADE20K. * denotes backbone pre-trained on the ImageNet-22k other than the ImageNet-1k, and training with 640×640 crop size.

Method	Backbone	Baseline	+HL
PSPNet [9]	ResNet-50 [5]	42.04	42.70 (+0.66)
PSPNet [9]	ResNet-101 [5]	44.60	45.20 (+0.60)
DeepLabV3+ [12]	ResNet-101 [5]	45.12	45.43 (+0.31)
UPerNet [41]	ResNet-101 [5]	44.02	44.55 (+0.53)
CCNet [22]	ResNet-101 [5]	44.26	44.61 (+0.35)
OCRNet [42]	HRNetV2P-W48 [53]	43.20	44.16 (+0.96)
UPerNet [41]	Swin-tiny [7]	43.50	43.98 (+0.48)
UPerNet [41]	Swin-Base [7]	50.25	50.95 (+0.70)
UPerNet* [41]	Swin-Base* [7]	51.29	52.52 (+1.23)
UPerNet* [41]	ConvNeXt-Base* [57]	52.17	52.96 (+0.79)

improves the baseline methods on categories of small-size objects (*e.g.*, traffic light, person, and rider) and with thin parts (*e.g.*, pole, motorcycle, and bicycle). These quantitative results show that the proposed method is effective in using various backbone networks for semantic segmentation.

Results of using different segmentation architectures: Since the pioneering FCN [8] for semantic segmentation, numerous fully convolutional semantic segmentation methods have been proposed. To further assess the effectiveness of the proposed method, we apply the proposed method on various popular segmentation architectures using the same ResNet-101 [5] backbone. As shown in Fig. 5, the proposed method also achieves consistent improvements ranging from 1.02% to 2.37% mIoU (1.49% mIoU on average) over all baseline methods. These results demonstrate that the proposed method can be applied to most segmentation methods and brings consistent improvements.

Experimental results on ADE20K: Since the experiment on ADE20K requires 160k iterations rather than 40k iterations for Cityscapes, we mainly conduct experiments by applying the proposed method to some classical segmentation methods using popular backbone networks (*e.g.*, ResNet-50/ResNet-101 [5], HRNet [53], Swin Transformer [7], and ConvNeXt [57]). As depicted in Tab. 3, the proposed method achieves consistent improvements (0.66% mIoU on average) over all baseline methods. In particular, applying the proposed method to UPerNet [41] with Swin Transformer [7] as

TABLE 4

Quantitative results of some methods on the validation set of iSAID.

Method	Backbone	Baseline	+HL
FCN [8]	HRNet-W18 (small) [53]	62.80	63.74 (+0.94)
FCN [8]	HRNet-W18 [53]	65.75	66.60 (+0.85)
PSPNet [9]	ResNet-18 [5]	60.76	62.93 (+2.17)
PSPNet [9]	ResNet-50 [5]	65.65	66.50 (+0.85)

TABLE 5

Quantitative results of some methods on the test set of Total-Text. The IoU score for the foreground text is depicted.

Method	Backbone	Baseline	+HL
FCN [8]	HRNet-W18 (small) [53]	66.62	68.56 (+1.94)
FCN [8]	HRNet-W18 [53]	69.32	70.58 (+1.26)
PSPNet [9]	ResNet-18 [5]	49.43	50.53 (+1.10)
PSPNet [9]	ResNet-50 [5]	52.91	53.93 (+1.02)

the backbone network achieves 1.23% mIoU improvement over the baseline method with relatively superior performance. The experimental results on ADE20K also demonstrate the effectiveness of the proposed method on various segmentation methods with different backbone networks.

Experiments on iSAID: Aerial images are usually acquired in top-down view, and are thus quite different from natural images. There are numerous small objects in the large-scale aerial images. Thus, it is quite challenging to segment high-resolution aerial images. We conduct experiments on the iSAID [3] for aerial image segmentation. Because of high-resolution images, following the common practice for this dataset, we simply conduct experiments using two popular segmentation methods with some compact backbones. The quantitative comparison with the baseline methods is depicted in Tab. 4. The proposed method achieves consistent improvements (1.20% mIoU on average) in segmenting aerial images, demonstrating the generality of the proposed method in segmenting various types of images.

Experiments on Total-Text: Finally, we evaluate the proposed method in segmenting scene texts on Total-Text [58]. Following the common practice, we report the IoU score of the foreground text (fgIoU) to quantitatively benchmark

TABLE 6

Quantitative results of using different pixel weight strategies in PSPNet [9] on Cityscapes validation set, using different backbones.

Method	PSPNet [9] with different backbone networks		
	ResNet-18	ResNet-50	ResNet-101
Cross-Entropy	74.30	78.68	79.60
Balanced CE	74.21	78.18	79.16
OHEM [26]	74.23	78.99	79.64
Focal loss [27]	73.35	78.43	78.95
HL (Ours)	75.60	79.58	80.65

TABLE 7

Quantitative results of setting different values for c involved in Eq. (1) on Cityscapes validation set, using different backbones for PSPNet [9].

Hyper-parameter c	PSPNet [9] with different backbone networks		
	ResNet-18	ResNet-50	ResNet-101
Baseline	74.30	78.68	79.60
$c = 0.01$	75.93 (+1.63)	79.39 (+0.71)	79.89 (+0.29)
$c = 0.1$	75.60 (+1.30)	79.58 (+0.90)	80.65 (+1.05)
$c = 0.5$	74.82 (+0.52)	79.04 (+0.36)	80.41 (+0.81)

different methods. We adopt the same baseline segmentation methods as experiments on iSAID for aerial image segmentation. The quantitative evaluation is depicted in Tab. 5, where we observe similar consistent performance improvements (1.33 fgIoU on average) for scene text segmentation. This further demonstrates the generality and effectiveness of the proposed method for semantic segmentation.

4.5 Ablation study

We conduct three types of ablation studies on Cityscapes: the effectiveness of using different pixel weights for pixel-wise cross-entropy segmentation loss, and the influence of the two hyper-parameters involved in Eq. (1) and Eq. (5).

Ablation study on different pixel weights: We mainly compare the proposed hardness level learning method with three types of pixel weights: 1) the balanced cross-entropy (Balanced CE) loss that weigh the classical cross-entropy loss based on the number of pixels in each category; 2) Cross-entropy loss with online hard example mining [26] (OHEM CE). Following the default setting in mmsegmentation [59], we set the probability threshold to 0.7 and keep at least 100,000 pixels for training; 3) Focal loss [27], for which we set the parameter γ to default value 2.

As depicted in Tab. 6, for the PSPNet [9] with different backbone networks, using the other three alternative pixel weights in cross-entropy segmentation loss does not perform well, and even sometimes performs worse than the baseline segmentation loss. This is not surprising and explains why they are not widely used in semantic segmentation. Indeed, as described in Sec. 3.1, the OHEM CE and focal loss are based on the current loss values. This may make the model over-fit to very few pixels which are ambiguous to distinguish, yielding degenerated segmentation results. On the other hand, the proposed hardness level

TABLE 8

Quantitative results of setting different values for α involved in Eq. (5) on Cityscapes validation set, using different backbones for PSPNet [9].

Hyper-parameter α	PSPNet [9] with different backbone networks		
	ResNet-18	ResNet-50	ResNet-101
Baseline	74.30	78.68	79.60
$\alpha = 0.001$	74.37 (+0.07)	78.69 (+0.01)	79.86 (+0.26)
$\alpha = 0.01$	75.60 (+1.30)	79.58 (+0.90)	80.65 (+1.05)
$\alpha = 0.1$	75.94 (+1.64)	79.62 (+0.94)	80.44 (+0.84)
$\alpha = 1$	75.82 (+1.52)	79.88 (+1.20)	80.16 (+0.56)

learning method achieves consistent performance improvement, showing the effectiveness of the proposed method.

Ablation study on hyper-parameter c in Eq. (1): This hyper-parameter c controls the maximum relative ratio between different pixels, helping to avoid overwhelming hardness level for a few pixels. A lower value for c implies focusing only on harder pixels for segmentation. We conduct an ablation study on c by setting it to 0.01, 0.1, and 0.5 for the PSPNet [9] with different backbone networks. As depicted in 7, the segmentation performance varies for different values of c , and is consistently better than the baseline method. This demonstrates that the proposed method is rather effective. Following the results of using the ResNet-101 backbone, we simply set c to 0.01 for all experiments. It is noteworthy that using a smaller value for c results in better segmentation performance improvement for the segmentation model with lightweight ResNet-18, which is less powerful than the cumbersome backbone in fitting the training samples. There are more hard pixels for the lightweight segmentation model. Therefore, using a smaller value of c for the lightweight segmentation backbone focuses more on harder pixels, yielding better results. In practice, we could adjust the value of c for different segmentation backbones to get better results.

Ablation study on hyper-parameter α in Eq. (5): This hyper-parameter controls the increasing rate of competing hardness level. We set α to 0.001, 0.01, 0.1, and 1 for PSPNet [9] with different backbone networks. As listed in Tab. 8, all settings of α improve the baseline method. For $\alpha \geq 0.01$, the proposed method achieves in general noticeable performance improvement for all backbone networks. Following the segmentation result with ResNet-101, we set α to 0.01 for all experiments.

4.6 Complexity analysis

The proposed hardness level learning for semantic segmentation is only involved during training. The performance improvements in Sec. 4.4 is achieved with no extra cost during the test phase. The proposed method only requires some extra cost in training. We give in Tab. 9 the extra cost in terms of relatively increased GPU memory usage for some segmentation methods on Cityscapes. As depicted in Tab. 9, the proposed method requires in general ignorable extra cost during training phase, which makes it easily applicable for most semantic segmentation methods.



Fig. 6. Qualitative illustration of some segmentation results on Cityscapes, ADE20K, iSAID, and Total-Text dataset (from top to bottom).

TABLE 9

Analysis of extra training cost (in terms of GPU memory usage) for the proposed method based on experiments on the Cityscapes dataset.

Method	Backbone	Increasing
NonLocal [13]		0.68%
PSPNet [9]		1.40%
DeepLabV3+ [12]	ResNet-101 [13]	4.26%
UPerNet [41]		12.11%
LRASPP [61]	MobileNetV3 [60]	0.01%
BiSeNetV2 [44]	BiSeNetV2 [44]	0.20%
PSPNet [9]	MobileNetV2 [54]	0.59%

TABLE 10

Quantitative results of applying the proposed method to U²PL [65] for semi-supervised semantic segmentation on Cityscapes validation set. "SupOnly" denotes the unlabeled images are not used for training. [†] stands for results from the original paper [65].

Method	Portion (number) of training images			
	1/16 (186)	1/8 (372)	1/4 (744)	1/2 (1488)
SupOnly [†]	65.74	72.53	74.43	77.83
U ² PL (w/CutMix) [†]	70.30	74.37	76.47	79.05
U ² PL (w/CutMix) +HL	71.11 72.62 (+1.51)	75.24 76.04 (+0.80)	75.86 76.55 (+0.69)	78.43 79.63 (+1.20)

4.7 Application to other segmentation tasks

Though the proposed method is mainly developed for fully-supervised semantic segmentation task, it can be easily applied to other segmentation tasks such as semi-supervised and domain-generalized semantic segmentation.

Semi-supervised semantic segmentation: Semi-supervised semantic segmentation aims to perform segmentation by making use of few labeled images and many unlabeled images. We conduct experiments of semi-supervised semantic segmentation on Cityscapes using state-of-the-art U²PL [65] as the baseline model. All the images in the training set of Cityscapes are used during training, but only a portion of the annotations of these training images are used. We compare the results under classical 1/16, 1/8, 1/4, and 1/2 partition protocols in semi-supervised semantic segmentation. As shown in Tab. 10, the proposed method also achieves consistent and noticeable performance improvements (1.05% mIoU) in semi-supervised semantic segmentation on Cityscapes. Note that we reproduce the results for U²PL using its official implementation for a fair comparison. This shows that the proposed method is also effective for semi-supervised semantic segmentation.

Domain-generalized semantic segmentation: To improve the segmentation performance for unseen domains, domain-generalized semantic segmentation (DG-Seg) has recently attracted much attention. We conduct a simple experiment to verify the effectiveness of the proposed method in DG-Seg task. Specifically, following the other DG-Seg methods [66], [68], [69], we adopt DeepLabV3+ [12] with ResNet-101 as the baseline model. We train both the baseline and the proposed method on the synthetic dataset GTAV [70],

TABLE 11

Quantitative benchmark of different domain-generalized semantic segmentation methods. "Extra data" denotes using extra real-world data during training. [†] denotes results from the original paper.

Method	Extra data	GTAV \Rightarrow Cityscapes
ISW [66] [†] (CVPR2021)	✗	37.09
FSDR [67] [†] (CVPR2021)	✓	44.80
WildNet [68] [†] (CVPR2022)	✗	45.79
SHADE [69] [†] (ECCV2022)	✗	46.66
DeepLabV3+ [12]	✗	36.56
+HL	✗	43.06 (+6.50)

and report segmentation results on the validation set of Cityscapes. As shown in Tab. 11, without bells and whistles, the proposed method achieves a 6.50% mIoU improvement over the baseline model in generalizing from synthetic GTAV to Cityscapes. The proposed method without any DG strategies achieves 43.06 mIoU, which is on par with some recent methods specifically designed for the DG-Seg task.

5 CONCLUSION

In this paper, we propose a novel pixel hardness learning method for semantic segmentation. Differently from existing hard pixel mining based on current loss values, the proposed pixel hardness learning makes use of global and historical loss values. This results in a stable and meaningful hardness level map related to inherent image structure, which generalizes well and helps in segmenting difficult areas. Applying the proposed pixel hardness learning method to many popular semantic segmentation methods achieves consistent/significant improvements on natural image segmentation, aerial and text image segmentation. Besides, the proposed method also improves the state-of-the-art semi-supervised semantic segmentation method, and demonstrates good generalization ability across domains. Note that the proposed method requires no extra cost during inference, and only slightly increases the training cost. In the future, we would like to explore the idea of pixel hardness learning for more applications, such as object detection and other dense prediction tasks.

REFERENCES

- [1] M. Cordts, M. Omran, S. Ramos, T. Rehfeld, M. Enzweiler, R. Benenson, U. Franke, S. Roth, and B. Schiele, "The Cityscapes dataset for semantic urban scene understanding," in *Proc. of IEEE Conf. on Computer Vision and Pattern Recognition*, 2016, pp. 3213–3223.
- [2] B. Zhou, H. Zhao, X. Puig, T. Xiao, S. Fidler, A. Barriuso, and A. Torralba, "Semantic understanding of scenes through the ADE20K dataset," *Intl. Journal of Computer Vision*, vol. 127, no. 3, pp. 302–321, 2019.
- [3] S. Waqas Zamir, A. Arora, A. Gupta, S. Khan, G. Sun, F. Shahbaz Khan, F. Zhu, L. Shao, G.-S. Xia, and X. Bai, "iSAID: A large-scale dataset for instance segmentation in aerial images," in *Proc. of IEEE Conf. on Computer Vision and Pattern Recognition Workshops*, 2019, pp. 28–37.
- [4] K. Simonyan and A. Zisserman, "Very deep convolutional networks for large-scale image recognition," in *Proc. of International Conference on Learning Representations*, 2015.
- [5] K. He, X. Zhang, S. Ren, and J. Sun, "Deep residual learning for image recognition," in *Proc. of IEEE Conf. on Computer Vision and Pattern Recognition*, 2016, pp. 770–778.

- [6] M. Tan and Q. Le, "EfficientNet: Rethinking model scaling for convolutional neural networks," in *Proc. of Intl. Conf. on Machine Learning*, 2019, pp. 6105–6114.
- [7] Z. Liu, Y. Lin, Y. Cao, H. Hu, Y. Wei, Z. Zhang, S. Lin, and B. Guo, "Swin transformer: Hierarchical vision transformer using shifted windows," in *Proc. of IEEE Intl. Conf. on Computer Vision*, 2021, pp. 10 012–10 022.
- [8] J. Long, E. Shelhamer, and T. Darrell, "Fully convolutional networks for semantic segmentation," in *Proc. of IEEE Conf. on Computer Vision and Pattern Recognition*, 2015, pp. 3431–3440.
- [9] H. Zhao, J. Shi, X. Qi, X. Wang, and J. Jia, "Pyramid scene parsing network," in *Proc. of IEEE Conf. on Computer Vision and Pattern Recognition*, 2017, pp. 2881–2890.
- [10] L.-C. Chen, G. Papandreou, I. Kokkinos, K. Murphy, and A. L. Yuille, "DeepLab: Semantic image segmentation with deep convolutional nets, atrous convolution, and fully connected CRFs," *IEEE Trans. on Pattern Anal. and Mach. Intell.*, vol. 40, no. 4, pp. 834–848, 2017.
- [11] L.-C. Chen, G. Papandreou, F. Schroff, and H. Adam, "Rethinking atrous convolution for semantic image segmentation," *arXiv preprint arXiv:1706.05587*, 2017.
- [12] L.-C. Chen, Y. Zhu, G. Papandreou, F. Schroff, and H. Adam, "Encoder-decoder with atrous separable convolution for semantic image segmentation," in *Proc. of European Conf. on Computer Vision*, 2018, pp. 801–818.
- [13] X. Wang, R. Girshick, A. Gupta, and K. He, "Non-local neural networks," in *Proc. of IEEE Conf. on Computer Vision and Pattern Recognition*, 2018, pp. 7794–7803.
- [14] H. Li, P. Xiong, J. An, and L. Wang, "Pyramid attention network for semantic segmentation," in *Proc. of British Machine Vision Conference*, 2018.
- [15] J. Fu, J. Liu, H. Tian, Y. Li, Y. Bao, Z. Fang, and H. Lu, "Dual attention network for scene segmentation," in *Proc. of IEEE Conf. on Computer Vision and Pattern Recognition*, 2019, pp. 3146–3154.
- [16] X. Li, Z. Zhong, J. Wu, Y. Yang, Z. Lin, and H. Liu, "Expectation-maximization attention networks for semantic segmentation," in *Proc. of IEEE Intl. Conf. on Computer Vision*, 2019, pp. 9167–9176.
- [17] J. He, Z. Deng, and Y. Qiao, "Dynamic multi-scale filters for semantic segmentation," in *Proc. of IEEE Intl. Conf. on Computer Vision*, 2019, pp. 3562–3572.
- [18] Z. Zhu, M. Xu, S. Bai, T. Huang, and X. Bai, "Asymmetric non-local neural networks for semantic segmentation," in *Proc. of IEEE Intl. Conf. on Computer Vision*, 2019, pp. 593–602.
- [19] Y. Cao, J. Xu, S. Lin, F. Wei, and H. Hu, "GCNet: Non-local networks meet squeeze-excitation networks and beyond," in *Proc. of IEEE Intl. Conf. on Computer Vision Workshops*, 2019, pp. 0–0.
- [20] L. Huang, Y. Yuan, J. Guo, C. Zhang, X. Chen, and J. Wang, "Interlaced sparse self-attention for semantic segmentation," *arXiv preprint arXiv:1907.12273*, 2019.
- [21] Z. Zhong, Z. Q. Lin, R. Bidart, X. Hu, I. B. Daya, Z. Li, W.-S. Zheng, J. Li, and A. Wong, "Squeeze-and-attention networks for semantic segmentation," in *Proc. of IEEE Conf. on Computer Vision and Pattern Recognition*, 2020, pp. 13 065–13 074.
- [22] Z. Huang, X. Wang, Y. Wei, L. Huang, H. Shi, W. Liu, and T. S. Huang, "CCNet: Criss-cross attention for semantic segmentation," *IEEE Trans. on Pattern Anal. and Mach. Intell.*, pp. 1–1, 2020.
- [23] M. Yin, Z. Yao, Y. Cao, X. Li, Z. Zhang, S. Lin, and H. Hu, "Disentangled non-local neural networks," in *Proc. of European Conf. on Computer Vision*, 2020, pp. 191–207.
- [24] Z. Li, Y. Sun, L. Zhang, and J. Tang, "CTNet: Context-based tandem network for semantic segmentation," *IEEE Trans. on Pattern Anal. and Mach. Intell.*, pp. 1–1, 2021.
- [25] Y. Liu, Y. Chen, P. Lasang, and Q. Sun, "Covariance attention for semantic segmentation," *IEEE Trans. on Pattern Anal. and Mach. Intell.*, vol. 44, no. 4, pp. 1805–1818, 2022.
- [26] A. Shrivastava, A. Gupta, and R. Girshick, "Training region-based object detectors with online hard example mining," in *Proc. of IEEE Conf. on Computer Vision and Pattern Recognition*, 2016, pp. 761–769.
- [27] T.-Y. Lin, P. Goyal, R. Girshick, K. He, and P. Dollár, "Focal loss for dense object detection," in *Proc. of IEEE Intl. Conf. on Computer Vision*, 2017, pp. 2980–2988.
- [28] X. Li, C. Lv, W. Wang, G. Li, L. Yang, and J. Yang, "Generalized focal loss: Towards efficient representation learning for dense object detection," *IEEE Trans. on Pattern Anal. and Mach. Intell.*, pp. 1–1, 2022.
- [29] D. Arpit, S. Jastrzebski, N. Ballas, D. Krueger, E. Bengio, M. S. Kanwal, T. Maharaj, A. Fischer, A. Courville, Y. Bengio et al., "A closer look at memorization in deep networks," in *Proc. of Intl. Conf. on Machine Learning*, 2017, pp. 233–242.
- [30] X. Li, Z. Liu, P. Luo, C. Change Loy, and X. Tang, "Not all pixels are equal: Difficulty-aware semantic segmentation via deep layer cascade," in *Proc. of IEEE Conf. on Computer Vision and Pattern Recognition*, 2017, pp. 3193–3202.
- [31] D. Wang, A. Haytham, J. Pottenburgh, O. Saeedi, and Y. Tao, "Hard attention net for automatic retinal vessel segmentation," *IEEE Journal of Biomedical and Health Informatics*, vol. 24, no. 12, pp. 3384–3396, 2020.
- [32] J. Yin, P. Xia, and J. He, "Online hard region mining for semantic segmentation," *Neural Processing Letters*, vol. 50, no. 3, pp. 2665–2679, 2019.
- [33] X. Deng, P. Wang, X. Lian, and S. Newsam, "NightLab: A dual-level architecture with hardness detection for segmentation at night," in *Proc. of IEEE Conf. on Computer Vision and Pattern Recognition*, 2022, pp. 16 938–16 948.
- [34] J. Chu, Y. Chen, W. Zhou, H. Shi, Y. Cao, D. Tu, R. Jin, and Y. Xu, "Pay more attention to discontinuity for medical image segmentation," in *Proc. of Intl. Conf. on Medical Image Computing and Computer Assisted Intervention*, 2020, pp. 166–175.
- [35] D. Nie and D. Shen, "Adversarial confidence learning for medical image segmentation and synthesis," *Intl. Journal of Computer Vision*, vol. 128, no. 10, pp. 2494–2513, 2020.
- [36] X. Hu, F. Li, D. Samaras, and C. Chen, "Topology-preserving deep image segmentation," *Proc. of Advances in Neural Information Processing Systems*, vol. 32, 2019.
- [37] X. Hu, Y. Wang, F. Li, D. Samaras, and C. Chen, "Topology-aware segmentation using discrete morse theory," in *Proc. of International Conference on Learning Representations*, 2021.
- [38] S. Chatterjee and P. Zielinski, "On the generalization mystery in deep learning," *arXiv preprint arXiv:2203.10036*, 2022.
- [39] S. Minaee, Y. Y. Boykov, F. Porikli, A. J. Plaza, N. Kehtarnavaz, and D. Terzopoulos, "Image segmentation using deep learning: A survey," *IEEE Trans. on Pattern Anal. and Mach. Intell.*, vol. 44, no. 7, pp. 3523–3542, 2022.
- [40] S. Zheng, S. Jayasumana, B. Romera-Paredes, V. Vineet, Z. Su, D. Du, C. Huang, and P. H. Torr, "Conditional random fields as recurrent neural networks," in *Proc. of IEEE Intl. Conf. on Computer Vision*, 2015, pp. 1529–1537.
- [41] T. Xiao, Y. Liu, B. Zhou, Y. Jiang, and J. Sun, "Unified perceptual parsing for scene understanding," in *Proc. of European Conf. on Computer Vision*, 2018, pp. 418–434.
- [42] Y. Yuan, X. Chen, and J. Wang, "Object-contextual representations for semantic segmentation," in *Proc. of European Conf. on Computer Vision*, 2020, pp. 173–190.
- [43] J. Liu, J. He, Y. Zheng, S. Yi, X. Wang, and H. Li, "A holistically-guided decoder for deep representation learning with applications to semantic segmentation and object detection," *IEEE Trans. on Pattern Anal. and Mach. Intell.*, pp. 1–1, 2021.
- [44] C. Yu, C. Gao, J. Wang, G. Yu, C. Shen, and N. Sang, "BiSeNet V2: Bilateral network with guided aggregation for real-time semantic segmentation," *Intl. Journal of Computer Vision*, vol. 129, no. 11, pp. 3051–3068, 2021.
- [45] Y. Yuan, L. Huang, J. Guo, C. Zhang, X. Chen, and J. Wang, "OCNet: Object context for semantic segmentation," *Intl. Journal of Computer Vision*, vol. 129, no. 8, pp. 2375–2398, 2021.
- [46] C. Yu, J. Wang, C. Peng, C. Gao, G. Yu, and N. Sang, "Learning a discriminative feature network for semantic segmentation," in *Proc. of IEEE Conf. on Computer Vision and Pattern Recognition*, 2018, pp. 1857–1866.
- [47] S. Borse, Y. Wang, Y. Zhang, and F. Porikli, "InverseForm: A loss function for structured boundary-aware segmentation," in *Proc. of IEEE Conf. on Computer Vision and Pattern Recognition*, 2021, pp. 5901–5911.
- [48] C. Wang, Y. Zhang, M. Cui, J. Liu, P. Ren, Y. Yang, X. Xie, X. Hua, H. Bao, and W. Xu, "Active boundary loss for semantic segmentation," in *Proc. of the AAAI Conf. on Artificial Intelligence*, 2022, pp. 2397–2405.
- [49] S. Zheng, J. Lu, H. Zhao, X. Zhu, Z. Luo, Y. Wang, Y. Fu, J. Feng, T. Xiang, P. H. Torr et al., "Rethinking semantic segmentation from a sequence-to-sequence perspective with transformers," in *Proc. of IEEE Conf. on Computer Vision and Pattern Recognition*, 2021, pp. 6881–6890.
- [50] E. Xie, W. Wang, Z. Yu, A. Anandkumar, J. M. Alvarez, and P. Luo, "SegFormer: Simple and efficient design for semantic segmentation with transformers," *Proc. of Advances in Neural Information Processing Systems*, vol. 34, pp. 12 077–12 090, 2021.
- [51] A. Krizhevsky, I. Sutskever, and G. E. Hinton, "ImageNet classification with deep convolutional neural networks," *Communications of the ACM*, vol. 60, no. 6, pp. 84–90, 2017.
- [52] S.-H. Gao, M.-M. Cheng, K. Zhao, X.-Y. Zhang, M.-H. Yang, and P. Torr, "Res2Net: A new multi-scale backbone architecture," *IEEE Trans. on Pattern Anal. and Mach. Intell.*, vol. 43, no. 2, pp. 652–662, 2019.

- [53] J. Wang, K. Sun, T. Cheng, B. Jiang, C. Deng, Y. Zhao, D. Liu, Y. Mu, M. Tan, X. Wang *et al.*, "Deep high-resolution representation learning for visual recognition," *IEEE Trans. on Pattern Anal. and Mach. Intell.*, vol. 43, no. 10, pp. 3349–3364, 2021.
- [54] M. Sandler, A. Howard, M. Zhu, A. Zhmoginov, and L.-C. Chen, "MobileNetV2: Inverted residuals and linear bottlenecks," in *Proc. of IEEE Conf. on Computer Vision and Pattern Recognition*, 2018, pp. 4510–4520.
- [55] A. Dosovitskiy, L. Beyer, A. Kolesnikov, D. Weissenborn, X. Zhai, T. Unterthiner, M. Dehghani, M. Minderer, G. Heigold, S. Gelly *et al.*, "An image is worth 16x16 words: Transformers for image recognition at scale," in *Proc. of International Conference on Learning Representations*, 2021.
- [56] H. Bao, L. Dong, S. Piao, and F. Wei, "BEiT: BERT pre-training of image transformers," in *Proc. of International Conference on Learning Representations*, 2022.
- [57] Z. Liu, H. Mao, C.-Y. Wu, C. Feichtenhofer, T. Darrell, and S. Xie, "A ConvNet for the 2020s," in *Proc. of IEEE Conf. on Computer Vision and Pattern Recognition*, 2022, pp. 11976–11986.
- [58] C. K. Ch'ng, C. S. Chan, and C. Liu, "Total-Text: Toward orientation robustness in scene text detection," *International Journal on Document Analysis and Recognition*, vol. 23, no. 1, pp. 31–52, 2020.
- [59] M. Contributors, "Mmsegmentation: Openmmlab semantic segmentation toolbox and benchmark," <https://github.com/open-mmlab/mmsegmentation>, 2020.
- [60] A. Howard, M. Sandler, G. Chu, L.-C. Chen, B. Chen, M. Tan, W. Wang, Y. Zhu, R. Pang, V. Vasudevan, Q. V. Le, and H. Adam, "Searching for MobileNetV3," in *Proc. of IEEE Intl. Conf. on Computer Vision*, 2019, pp. 1314–1324.
- [61] A. Howard, A. Zhmoginov, L.-C. Chen, M. Sandler, and M. Zhu, "Inverted residuals and linear bottlenecks: Mobile networks for classification, detection and segmentation," 2018.
- [62] S. Xie, R. Girshick, P. Dollár, Z. Tu, and K. He, "Aggregated residual transformations for deep neural networks," in *Proc. of IEEE Conf. on Computer Vision and Pattern Recognition*, 2017, pp. 1492–1500.
- [63] H. Zhang, C. Wu, Z. Zhang, Y. Zhu, H. Lin, Z. Zhang, Y. Sun, T. He, J. Mueller, R. Manmatha *et al.*, "ResNeSt: Split-attention networks," in *Proc. of IEEE Conf. on Computer Vision and Pattern Recognition Workshops*, 2022, pp. 2736–2746.
- [64] Z. Wang, A. C. Bovik, H. R. Sheikh, and E. P. Simoncelli, "Image quality assessment: from error visibility to structural similarity," *IEEE Trans. on Image Processing*, vol. 13, no. 4, pp. 600–612, 2004.
- [65] Y. Wang, H. Wang, Y. Shen, J. Fei, W. Li, G. Jin, L. Wu, R. Zhao, and X. Le, "Semi-supervised semantic segmentation using unreliable pseudo-labels," in *Proc. of IEEE Conf. on Computer Vision and Pattern Recognition*, 2022, pp. 4248–4257.
- [66] S. Choi, S. Jung, H. Yun, J. T. Kim, S. Kim, and J. Choo, "RobustNet: Improving domain generalization in urban-scene segmentation via instance selective whitening," in *Proc. of IEEE Conf. on Computer Vision and Pattern Recognition*, 2021, pp. 11580–11590.
- [67] J. Huang, D. Guan, A. Xiao, and S. Lu, "FSDR: Frequency space domain randomization for domain generalization," in *Proc. of IEEE Conf. on Computer Vision and Pattern Recognition*, 2021, pp. 6891–6902.
- [68] S. Lee, H. Seong, S. Lee, and E. Kim, "WildNet: Learning domain generalized semantic segmentation from the wild," in *Proc. of IEEE Conf. on Computer Vision and Pattern Recognition*, 2022, pp. 9936–9946.
- [69] Y. Zhao, Z. Zhong, N. Zhao, N. Sebe, and G. H. Lee, "Style-hallucinated dual consistency learning for domain generalized semantic segmentation," in *Proc. of European Conf. on Computer Vision*, 2022.
- [70] S. R. Richter, V. Vineet, S. Roth, and V. Koltun, "Playing for data: Ground truth from computer games," in *Proc. of European Conf. on Computer Vision*, 2016, pp. 102–118.